Cellulose (2017) 24:295–309
DOI 10.1007/s10570-016-1079-7

ORIGINAL PAPER

Engineering microfluidic papers: determination of fibre source and paper sheet properties and their influence on capillary-driven fluid flow

Franz Carstens · José A. F. Gamelas · Samuel Schabel

Received: 11 April 2016 / Accepted: 26 September 2016 / Published online: 20 October 2016

Abstract In the present study, the surface chemistry of fibres from different sources (groundwood, cotton linters, eucalyptus sulphate and a mixture of pine sulphate and spruce sulphate) was initially assessed via inverse gas chromatography. Significant differences were revealed among the four fibre types, especially between groundwood and the other three with regard to the surface energy and to the specific component of the work of adhesion of different polar probes. Moreover, the freeness value and the specific surface area of the diverse fractionated and unfractionated fibrous materials were investigated. In addition, the porosity and the pore size distribution of lab engineered paper sheets produced with the previously mentioned fibre sources were studied while modifying the fibre length and grammage. Novel approaches to modulate and control fluid transport in the lab-engineered paper substrates were introduced by using different fibre sources with the same freeness value, by fractionating the fibres before fabricating the paper substrates, and by changing the orientation of the fibres. The experimental results for our lab-engineered paper substrates and commercially available filter paper were compared with each other. Our findings suggest a considerable improvement in liquid transport velocity of tailor-made microfluidic paper based analytical devices with lab-engineered paper substrates. By altering the mentioned fibre and paper values, we managed to reduce or raise the capillary rise, which eventually allows us to modulate and control fluid flow in a more accurate and desirable way. Finally, changes in the fluid transport for paper substrates laid on materials with different water contact angles were tested. The obtained information thereby provides an alternative method to increase or decrease the capillary rise.

Keywords Paper-based microfluidics · Fluid transport · Inverse gas chromatography · Mercury intrusion porosimetry · Capillary rise · Contact angle · Specific surface area

F. Carstens (✉) · S. Schabel
Chair of Paper Technology and Mechanical Process Engineering, Technische Universität Darmstadt, 64283 Darmstadt, Germany
e-mail: carstens@papier.tu-darmstadt.de

J. A. F. Gamelas
Chemical Process Engineering and Forest Products Research Centre, University of Coimbra, 3030-790 Coimbra, Portugal

Introduction

Paper has been used as a substrate material for over 200 years, when scientific reports of litmus paper as a medium for analytical testing of chlorine and carbonic oxide were published (Davy 1812). The first paper-based microfluidics was invented by Müller and Clegg (1949) almost 150 years later,

when they conducted a mixture of pigments in a restricted channel on filter paper. However, it was the Whitesides' Group of Harvard University that in 2007 made paper-based microfluidics by introducing a patterned paper as a platform for portable bioassays (Martinez et al. 2007). Since then, over 1000 articles in the field of microfluidic paper-based analytical devices (μPADs) have been published (Cate et al. 2015). In addition, paper has gained great interest as a substrate material for electronics (Nguyen et al. 2014; Tobjörk and Österbacka 2011). The main reason why paper has become a very attractive substrate for making μPADs is due to its numerous advantages: (1) paper consists of cellulose, which is a very cheap and renewable material; (2) it does not necessarily need external forces for fluid transport thanks to capillary forces; and (3) it has an extraordinary compatibility with chemical and biochemical applications, which heightens the possibilities for specific functions and fabrication techniques (Böhm et al. 2014; Li et al. 2012). Besides cellulose, micro-nano fibrillated cellulose (MNFC) or regenerated cellulose manufactured by spin-coating of trimethylsilyl cellulose are other cellulose based materials suited for the creation of patterns (Kämäräinen et al. 2016; Kargl et al. 2013).

The basic principle for fabricating μPADs is to create capillary channels inside paper substrates that are able to control the fluid flow. According to literature, there are several techniques for fabricating μPADs: (1) flexography printing (Olkkonen et al. 2010), (2) ink jet etching (Abe et al. 2008, 2010), (3) ink jet printing (Delaney et al. 2011; Li et al. 2010), (4) laser treatment (Chitnis et al. 2011), (5) paper cutting (Fenton et al. 2009; Wang et al. 2010), (6) photolithography (Martinez et al. 2007, 2008), (7) plasma treatment (Li et al. 2008), (8) plotting with an analogue plotter (Bruzewicz et al. 2008), (9) screen printing (Dungchai et al. 2011), and (10) wax printing (Carrilho et al. 2009; Lu et al. 2010; Taudte et al. 2013). These techniques rely on creating hydrophilic-hydrophobic barriers to shape the desired channels; either by blocking the paper pores, depositing a hydrophobizing reagent on the fibre's surface, or by chemically modifying the fibre's surface (Li et al. 2012). Only one technique relies on a different method; paper cutting merely consists in shaping paper pattern by cutting and folding it.

The first researchers who studied the dynamics of capillary flow were Poiseuille (1828), Lucas (1918), and Washburn (1921). They found a linear relation between the wicking rate and the square root of time, by not taking the inertial and gravitational forces into consideration (Masoodi et al. 2010). This model, known as the Washburn equation (first order), also assumed parallel, cylindrical capillaries with homogeneous radii, as well as a laminar flow and an incompressible fluid, chemical homogeneity, and unlimited reservoir volume (Cate et al. 2015). Furthermore, the capillary's length is much longer than its width (Washburn 1921).

Several research groups have since presented modified equations to improve the predictive accuracy of fluid flow. Szekely et al. (1971) widened the model by taking inertial and gravitational forces into account. Cai et al. (2010) extended Washburn's equation to characterize the process of water absorption in a porous medium. Some efforts have been made to characterize fluid flow in heterogeneous cross sections (Bal et al. 2011; Reyssat et al. 2008; Shou et al. 2014; Xiao et al. 2012). Mark et al. (2012) stated that accurately estimating the capillary radius is essential for closely understanding and describing wicking phenomena. Fang et al. (2014) recently developed a non-uniform capillary model for unidirectional fibre bundles considering pore size distribution, which disagrees with previous works that considered mean pore values (Masoodi et al. 2007; Patro et al. 2007). Fu et al. (2010, 2011) showed that the flow rate of a fluid within a paper strip of constant width depends on the resistance established by the wet paper behind the fluid front. In addition, they revealed that by changing the width of a paper strip, a similar control of the fluid transport can be modulated. Another interesting finding is that dissolvable barriers can also be used as flow modulators, which are capable of decelerating the fluid flow in specific segments of the paper network (Lutz et al. 2013). A later study of the fluid transport in paper channels defined by hydrophobic barriers revealed lowered flow rates, when the width of the paper channel is smaller than the length of the cellulose fibres used during paper sheet moulding (Böhm et al. 2014).

Although vast research and considerable progress in the principle of fluid flow using paper-based substrates has been extensively made, little work has focused on studying and understanding parameters of paper itself

that may alter the fluid transport in μPADs. To date, many research groups have centred their strategies on using simple commercially available filter paper (Böhm et al. 2014; Cate et al. 2015; Li et al. 2012). Some of them have studied parameters of the cellulosic materials such as the fibre type and grammage used during paper fabrication (Guan et al. 2014; Li et al. 2014; Nilghaz et al. 2015). Nevertheless, there still are many parameters, like the fibre's length and orientation, which have not been tested at all. In addition, the knowledge of the swelling and absorption properties of fibres in an aqueous environment may lead to a better control and manipulation of the fluid transport in microfluidic papers. With this knowledge, better and accurate μPADs may be fabricated, since the manipulation of the fluid flow is of great interest and importance for biomedical and environmental applications. Even more, the functionality of the devices as well as their performance can be greatly improved.

In this paper, we introduce alternative ways of manipulating fluid transport in paper strips by altering and testing both fibre and paper properties. Four different fibre types were considered: groundwood, cotton linters, eucalyptus kraft pulp, and a mixture of 50 % pine and 50 % spruce kraft pulp. Each fibre type was specifically selected for this study: groundwood, with high lignin content; cotton linters, a nonwood fibre; eucalyptus, a hardwood; and the mixture of pine and spruce, a combination of softwoods. These were firstly characterized for their physico-chemical surface properties by means of inverse gas chromatography. Simultaneously, these fibres were beaten in order to reach an equal freeness level. After that, some samples were fractionated in order to test the influence of the fibre's length. Later, the specific surface area of all samples was determined with the Pulmac permeability method. Then, conventional lab-engineered paper sheets with established grammages were formed. Concurrently, anisotropic lab-engineered paper sheets with a MK sheet former series 9000 were made, to define discrepancies between the isotropic and anisotropic sheet formation. In addition, all paper sheets were tested for their porosity and pore size distribution using mercury intrusion porosimetry, followed by determining the capillary rise as a function of time according to the Klemm method (ISO 8787) or with help of microscope images. Finally, all results were compared to determine the overall tendencies.

Experimental

Materials

For this work four different fibre sources were used: groundwood (GW, unbleached), cotton linters (CL, bleached), eucalyptus sulphate (ES, bleached), and a long fibre sulphate mixture (LFS, 50 % pine sulphate, 50 % spruce sulphate, bleached). In addition, Macherey–Nagel No. 4 filter paper (grammage: 80 g/m^2) was used. Moreover, deionised water and mercury (≥98 %, Roth) for the Klemm method and the mercury intrusion porosimetry were used accordingly. Finally, a small piece of glass, a steel plate and Parafilm M tape were used for the microscope image analysis.

Inverse gas chromatography (IGC) analysis

The main purpose of the IGC is to analyse a solid material for its physico-chemical surface properties. This technique enables to determine the dispersive component of the surface energy, adsorption thermodynamic parameters with a wide range of polar substances, Lewis acid–base character of the surface, surface nanoroughness parameter, among other relevant information (Gamelas 2013; Gamelas et al. 2014; Mukhopadhyay and Schreiber 1995; Santos and Guthrie 2005). It is advantageous over the classical contact angle measurements for the analysis of porous, rough, heterogeneous and hydrophilic materials; such is the case of cellulosic samples.

Unbleached groundwood, as well as bleached cotton linters, eucalyptus sulphate and long fibre sulphate pulps were previously milled with a Retsch ball mill S1000 for 36 min. The IGC analysis was done using a DANI GC 1000 digital pressure control gas chromatograph equipped with a hydrogen flame ionization detector. Stainless-steel columns, 0.5 m long and 0.4 cm inside diameter were washed with acetone and dried before packing. For each analysis, approximately 1–2 g of fibres was packed into the gas chromatograph column. The columns were shaped in a smooth ''U" to fit the detector/injector geometry of the instrument. The packed columns were conditioned overnight at 378.15 K, under a helium flow, before any measurements were made. Measurements were carried out at the column temperature of 313.15 K with the injector and detector kept at 453.15 K and

473.15 K, respectively. Helium was used as a carrier gas with a flow rate that in each material was optimized in order to have a good separation between the retention times of the different probes. Small quantities of probe vapour (<1 µl) were injected into the carrier gas, allowing work under infinite dilution conditions. The probes used for the IGC data collection were *n*-pentane, *n*-hexane, *n*-heptane, *n*-octane, *n*-nonane, trichloromethane (TCM, Lewis acidic probe), tetrahydrofurane (THF, basic), ethyl ether (basic), ethyl acetate (ETA, amphoteric) and acetone (amphoteric). All probes were of chromatographic grade and were used as received (Sigma-Aldrich). Methane was used as the reference probe. The retention times were the average of three injections and were determined by the Conder and Young method (Kamdem and Riedl 1992) due to the asymmetry of some chromatograms. The coefficient of variation between runs of retention time measurements was always below 5 %, being obtained higher variations for polar probes.

The principles and theoretical aspects of inverse gas chromatography can be found elsewhere (Gamelas 2013; Mukhopadhyay and Schreiber 1995; Santos and Guthrie 2005). In this work, using this technique, the dispersive component of the surface free energy of the solid materials (γ_s^d) and the specific component of the work of adhesion (W_a^s) of the several aforementioned polar probes with different acid–base properties on the materials surface were assessed.

Shortly, the dispersive component of the surface energy of each analysed material was estimated following the Schultz and Lavielle approach (Schultz et al. 1987), i.e., from the slope of the linear fit of $RT\ln(V_n)$ as a function of $2N \times a(\gamma_l^d)^{0.5}$ (Eq. 1) using the IGC data obtained with the apolar probes. Here, V_n is the net retention volume (which is calculated from the retention time of the injected probe through the column), T is the column absolute temperature, R is the gas constant, N is the Avogadro number, a is the molecular surface area of the probe, γ_l^d is the dispersive component of the surface free energy of the probe. The constant K is dependent on the chosen reference state.

$$RT\ln(V_n) = \sqrt{\gamma_s^d}2N \times a\sqrt{\gamma_l^d} + K \quad (1)$$

The specific component of the free energy of adsorption (ΔG_a^s) of each polar probe was calculated based on Eq. (2), i.e. by the difference between the experimental value of $RT\ln(V_n)$ obtained for the polar probe and the corresponding estimation for the equivalent apolar probe based on the linear fitting of $RT\ln(V_n)$ versus $2N \times a(\gamma_l^d)^{0.5}$ for *n*-alkanes (reference line).

$$\Delta G_a^s = -RT\ln\frac{V_n}{V_{n,ref}} \quad (2)$$

The specific component of the work of adhesion (W_a^s) was then calculated from the ΔG_a^s parameter, according to Eq. (3).

$$W_a^s = -\frac{\Delta G_a^s}{N.a} \quad (3)$$

Note that the properties assessed by IGC, besides giving relevant information about the fibres surface characterization, could provide also useful information for the understanding of phenomena related to wetting and penetration if these are driven not only by physical but also by chemical characteristics of the fibres.

Preparation of pulp fractions and lab-engineered paper sheets

For the preparation of the pulp fractions and the lab-engineered paper substrates, unbleached groundwood, bleached eucalyptus sulphate, a mixture of 50 % pine sulphate and 50 % spruce sulphate, and cotton linters were used. The fibres were refined in a Voith LR 40 laboratory refiner with effective specific energies of 300, 150, 175, and 200 kWh/t, respectively, in order to obtain a freeness value of 36 ± 1 SR. The chosen milling sets for the refining were: 2/3-1.42-60 for ES, 3/3-1.0-60 for LFS and GW, and 3/3-1.0-60 conic for CL. The freeness value was determined according to ISO 5267. Afterwards, the three bleached pulps were fractionated with a Haindl-McNett fractionator according to the Zellcheming code of practice V/1.4/86. Four different filters (R14, R30, R50 and R200) with different mesh sizes (1.18, 0.6, 0.3 and 0.075 mm) were used to perform this task, whereat the filter with the largest mesh size was merely used as a prefilter to separate very large fibres and foreign materials. Important to mention is that a part of the pulp was neither beaten nor fractionated. The reason

behind this was to have untreated pulp, which could be used as reference for further studies.

Once the refining and the fractionation were completed, a series of lab-engineered paper sheets, consisting of isotropically layered cellulose fibres was fabricated on a conventional Rapid-Koethen hand-sheet mould (ISO 5269/2). In addition, a series of lab-engineered paper sheets, consisting of anisotropically layered cellulose fibres was fabricated on a M/K series 9000 automated sheet former. For both fabrication techniques paper sheets with grammages of 40 ± 1, 60 ± 1, 80 ± 1, and 100 ± 1 g/m^2 were formed. The grammages were determined according to ISO 536:2012. Furthermore, all paper substrates were stored at a temperature of 296.15 ± 1 K and a relative humidity of 50 ± 2 % for a minimum of 24 h, before further characterization was performed. During this period of time, the paper substrates reached an equilibrium containing 5.25 ± 0.25 % water, which was absorbed from the humid air.

Pulmac permeability test

The specific surface area of cotton linters, eucalyptus fibres and long fibre mixture was determined with the Pulmac permeability test developed by Pulmac Research Ltd, which is based on the principles of Robertson and Mason (1949) with certain modifications to improve accuracy and speed. Apart from the specific surface area, this method also determines the specific volume, wet permeability and compressibility of the fibres (Singh 2007).

In order to determine the specific surface area, Robertson and Mason (1949) rearranged the modified Kozeny–Carman equation (Carman 1937, 1956; Kozeny 1927) into the form,

$$\left(K \cdot c^2\right)^{\frac{1}{3}} = \left(\frac{1}{k \cdot S}\right)^{\frac{1}{3}} \cdot (1 - v \cdot c) \tag{4}$$

where K is the permeability coefficient, c is the apparent density, k is the Kozeny–Carman constant, S is the specific surface area, and v is the specific volume. This equation gives a linear relation between $(K \cdot c^2)^{\frac{1}{3}}$ and c, assuming that the fluid flow through the pulp mat is laminar, and that the specific surface area and specific volume are independent of the pulp mat density (Rudman and Patterson 1998). By plotting the equation with a k value of 5.55 for fibre pulp, the specific surface area is given from the intercept, just as the specific volume is given from the slope of the line (Singh 2007). The idea behind measuring the specific surface area was to find a correlation with the porosity through the freeness; the porosity and the freeness correlate to one another. If the specific surface area shows a correlation with the freeness, a connection between the specific surface area and the porosity may be established.

Mercury porosimetry analysis

The mercury porosimetry is an analytical technique, which is based on the intrusion of mercury into a porous structure under strictly controlled pressure (Micromeritics 2015). The measurement principle applies the Washburn equation, which establishes a relationship between the pores diameter and the pressure (León y León 1998; Webb 2001).

This analysis was conducted with a Micromeritics AutoPore IV 9500 mercury porosimeter according to the standard operating procedure (Sieb 2015), in order to measure the porosity and pore size distribution of the paper substrate samples, by increasing a controlled pressure in fine increments from 0.01 to 227 MPa. The equilibrium time for each pressure point was 30 s. All samples were fabricated as described in section "Preparation of pulp fractions and lab-engineered paper sheets". Afterwards, paper strips with a width of 15 mm were cut. The length of the samples varied so that each sample weighed 1.5 g. Then the samples were placed into a penetrometer assembly (part no. 950.61707.00).

After the measurement, the provided software of the mercury porosimeter delivered the results for the porosity and mean pore size. The results for the pore size distribution were calculated separately with Office Excel 2010.

Important to mention is that the porosity ϕ was not only determined with the mercury porosimetry analysis, but it also was calculated with the following equation,

$$\phi = \frac{V_v}{V_t} = 1 - \frac{\rho_p}{\rho_c} \tag{5}$$

where V_v is the void volume of a paper sample, V_t is the total volume of the paper sample, ρ_p is the density of the paper sample, and ρ_c is the density of cellulose, which has a value of 1.53 g/cm^3 (Niskanen 1998). The main

reason for the calculation of the porosity is to compare the results with those of the mercury porosimetry analysis and establish the measuring inaccuracy of this method due to its limitations and flaws. One of the most important ones is the fact that it measures the largest entrance towards a pore and not the actual inner size of a pore (Giesche 2006). Furthermore, the high pressures applied in this technique to the samples may change or damage their structure, since paper is after all a compressible material.

Determination of capillary rise

The capillary rise of different lab-engineered paper substrates made from groundwood, cotton linters, eucalyptus sulphate, LFS, and of common filter paper was determined according to the Klemm method (ISO 8787). This method estimates the capillary rise after 10 min. However, in order to precisely observe the changes in the capillary rise as a function of time, they were recorded with a video camera during the whole 10 min.

For the purpose of determining the capillary rise of paper substrates, when the paper samples are in direct contact with another material, high resolution images with a Zeiss Stemi 2000-C microscope were taken with an interval of 4 s. For this analysis, the following materials were utilized: a piece of glass, a steel plate, and a Parafilm M tape. Paper strips with a width of seven mm were placed on the materials. Then 20 ml of deionised water were dropped on the paper. After 5 s, the measurement started, giving water time to penetrate into the sample. Finally, up to nine images were taken, showing the progress of the water front in the paper strips.

It is important to mention that all capillary rises were measured at a temperature of 296.15 ± 1 K and a relative humidity of 50 ± 2 %.

The contact angles were measured with a Dataphysics Instruments contact angle analyzer, model OCA 35. Figure 1 shows the water contact angles of the three tested samples; glass (left), steel (middle), and Parafilm tape (right). Each sample presented a different contact angle; glass with a water contact angle of 27.5°, steel with a water contact angle of 76°, and the Parafilm M tape with a water contact angle of 111°. The contact angle of the paper substrate could not be measured with this method due to its high wettability. The contact angle of untreated pulp is indeed very difficult to determine (Hubbe et al. 2015). Many authors have measured it with different techniques; however, they all have reached different values, from 0° to 35° (Erbil 1997; Hodgson and Berg 1988; Joubert et al. 1959; Liukkonen 1997; Wistara and Young 1999). Therefore, we won't focus on this value, but in the influence of combined materials on the capillary rise.

Results and discussion

First, differences in the chemical surface properties between unbleached groundwood, the bleached cotton linters, eucalyptus sulphate and LFS samples were investigated using IGC. The results obtained for the dispersive component of the surface energy and the specific components of the works of adhesion of several polar probes are summarized in Table 1. The ratios W_a^s(THF)/W_a^s(TCM) and W_a^s(ether)/W_a^s(TCM), that give an indication of the prevalence of the Lewis acidity over the Lewis basicity of the material surface, are also presented in the last columns (as mentioned, THF and ethyl ether are Lewis basic probes while TCM is a Lewis acidic probe). It is known that only the highest-energy sites of the surface are measured by the IGC technique under infinite dilution conditions and thus somewhat overestimated results can be obtained for some of the parameters. Notwithstanding, it is often the interaction with these sites of the material surface that matters and accordingly the obtained results are of high relevance.

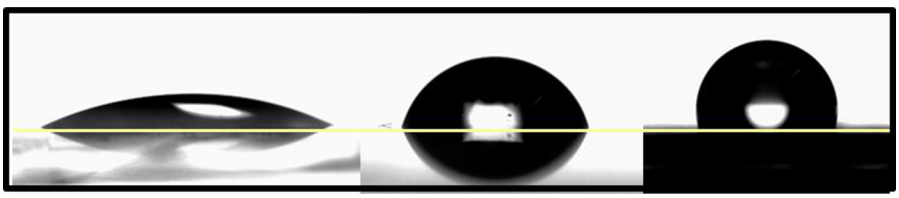

Fig. 1 Water contact angle of glass (*left*), steel (*middle*) and Parafilm tape (*right*)

Table 1 Dispersive component of the surface energy (γ_s^d, mJ/m^2) and specific component of the work of adhesion (W_a^s, mJ/m^2) of polar probes for the cellulosic samples

Sample	γ_s^d	W_a^s (TCM)	W_a^s (THF)	W_a^s (ether)	W_a^s (acetone)	W_a^s (ETA)	$\frac{W_a^s(THF)}{W_a^s(TCM)}$	$\frac{W_a^s(ether)}{W_a^s(TCM)}$
Eucalyptus sulphate	44.0	5.1	22.6	17.2	31.2	23.9	4.5	3.4
LFS mixture	48.4	5.2	23.1	20.2	32.3	23.8	4.4	3.9
Cotton linters	46.0	4.7	25.7	22.1	36.8	27.2	5.5	4.7
Groundwood	36.7	4.9	7.9	3.2	16.1	7.3	1.6	0.7

Parameters were determined at 313.15 K. Errors associated to the determinations are typically <5 % for the γ_s^d and <2 % for the W_a^s values

For groundwood, the dispersive component of the surface energy showed the lowest value. Additionally, the ratios W_a^s(THF)/W_a^s(TCM) and W_a^s(ether)/W_a^s(TCM) were also the lowest for groundwood (lower acidity to basicity ratio) due to the significantly lower W_a^s(THF) and W_a^s(ether). The surface of groundwood also showed much lower specific affinity for amphoteric probes (acetone and ETA, which also show a high degree of Lewis basicity). These behaviours are most probably related to the presence of lignin and extractives in the groundwood sample which typically have lower γ_s^d, lower affinity for polar probes and are more bipolar type (Shen and Parker 1999).

On the other hand, ES, LFS and CL showed γ_s^d values in the range expected for cellulosic materials (40–50 mJ/m^2 at 303–313 K) (Carvalho et al. 2005; Gamelas et al. 2011; Gamelas 2013; Reutenauer and Thielmann 2003; Shen et al. 1998). The differences between the different materials were not larger than 4 mJ/m^2, suggesting that they present comparable behaviour regarding γ_s^d. The surface of these materials showed a prevalence of the Lewis acidity over the Lewis basicity, as demonstrated by the W_a^s(THF)/W_a^s(TCM) and W_a^s(ether)/W_a^s(TCM) ratios (in the range of 3.4–5.5). Higher specific interactions were observed with amphoteric (acetone, ETA) and basic (THF, ether) probes, as common behaviour for cellulosics (Gamelas 2013). However, while for eucalyptus and LFS mixture, the corresponding specific interactions were similar (except for the W_a^s(ether)), significantly higher specific interactions with basic and amphoteric probes and, accordingly, higher W_a^s(THF)/W_a^s(TCM) and W_a^s(ether)/W_a^s(TCM) ratios were found for cotton linters. This result indicates a higher exposure of cellulose molecules, that are more Lewis acidic than Lewis basic, in the surface of bleached cotton fibres which will thus provide higher specific interactions with those probes possessing a more basic character (including the amphoteric ETA and acetone probes that are more Lewis basic than Lewis acidic). Note that, even in bleached cellulosic pulps or pure cotton cellulose, other components such as fatty acids and waxes are present on the surface of the fibres, as widely reported using X-ray photoelectron spectroscopy (Shen et al. 1998; Topalovic et al. 2007), which also influence the surface chemistry. Overall, it can be concluded that the four cellulosic fibre types studied here, do not have exactly the same surface chemistry. In particular, groundwood is clearly distinguished from LFS mixture, cotton linters and eucalyptus sulphate fibres for its surface properties.

After the IGC analysis was completed, the work was continued with the study of the freeness and specific surface area of the cellulosic pulps. Tables 2, 3, and 4 show the results obtained for cotton linters, LFS mixture and eucalyptus sulphate, respectively. Each table first shows the freeness value with its corresponding standard deviation value (SD_F); followed by the specific surface area value, also with its matching standard deviation value (SD_S). Finally, the correlation coefficient value between the freeness and specific surface area of all samples is shown. It is important to mention that the freeness value was determined twice, as established in ISO 5267; while the specific surface area was determined thrice.

The freeness and specific surface area values for all pulps were different, yet congruent. In all cases the largest fibre length (R30) presented the lowest values. As the fibre length (R50, R200) gets smaller, so do freeness and specific surface area values get higher. Johansson, among others, investigated the relationship between fibre length and freeness value (Johansson

Table 2 Freeness and specific surface area of cotton linters pulp fractions

Fraction	Freeness SR	SD_F	Spec. surface area (m^2/g)	SD_S	Correlation coefficient
R30	14	0.70	0.69	0.06	0.96
R50	15	0.01	0.73	0.01	
R200	20	0.01	1.09	0.09	
Unfractionated	36	0.70	2.76	0.09	

Table 3 Freeness and specific surface area of long fibre sulphate pulp fractions

Fraction	Freeness SR	SD	Spec. surface area (m^2/g)	SD	Correlation coefficient
R30	15.5	0.70	0.81	0.10	0.93
R50	17	0.02	1.31	0.11	
R200	28	1.40	2.70	0.10	
Unfractionated	37	1.73	3.02	0.14	

Table 4 Freeness and specific surface area of eucalyptus sulphate pulp fractions

Fraction	Freeness SR	SD	Spec. surface area (m^2/g)	SD	Correlation coefficient
R30	17	0.02	0.91	0.07	1.0
R50	18.5	0.02	1.04	0.06	
R200	19	1.00	1.16	0.14	
Unfractionated	36	0.40	2.82	0.48	

2011), which agrees with the acquired results. As for the specific surface area, this relation can be explained due to the fibre size itself, as well as due to the pore sizes. However, the highest values were measured with unfractionated pulp, where fibre lengths are mixed.

Once the lab-engineered paper sheets were formed, their porosity was measured. Figure 2 shows the results of the porosity as a function of the grammage for the three fibre types with equal fibre length (R50). It can be observed that each fibre type presents a different porosity; LFS mixture having the smallest value, followed by eucalyptus sulphate. The highest porosity values were obtained with cotton linters. All fibre types show the highest value at a grammage of

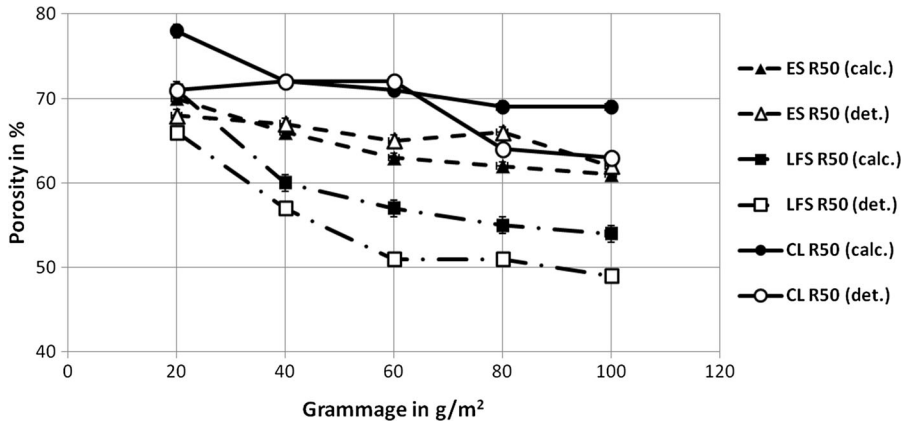

Fig. 2 Porosity over grammage for eucalyptus fibres (ES), long fibre mixture (LFS), and cotton linters (CL). Results determined (det.) by mercury porosimetry analysis, and calculated (calc.) with Eq. (5)

20 g/m^2. As the grammage increases, the porosity slightly decreases, reaching a minimum value at 100 g/m^2. In addition, the values for the calculated porosity and the determined porosity present a relative variation. In most of the cases, the calculated values are higher than the determined ones; the values vary up to eight per cent to one another. This inaccuracy can be explained due to a compression of the sample due to high pressures during the mercury porosimetry analysis. Also, the different shape of the pores cannot be completely measured; i.e. mercury intrusion porosimetry is not able to measure closed or blind pores. Both arguments explain the decrease in the porosity from the calculated values. Nevertheless, all results present a similar gradient and the same influence to this anomaly. It is important to mention that the same tendencies were observed with other fibre lengths.

Analogously to the porosity measurement, the pore size distribution was also determined by means of mercury porosimetry analysis. Figure 3 shows an example of the pore size distribution (or differential intrusion) for the different fibre types at a grammage of 80 g/m^2. Overall the pore sizes of the samples are in the same interval. However, there are notorious trends regarding each fibre type. CL presents a common Gaussian distribution with slight fluctuations. Despite of looking much CL alike, ES exhibits a second little peak at bigger pore sizes. An extreme case is presented by LFS, which shows two different peaks with almost the same probability. This behaviour suggests the first peak (left) shows the pore sizes of the fibre pores themselves, while the second peak (right) reveals the pore sizes of the voids between fibres. In general, if the pore sizes of fibres and void volumes are similar, then the course of the curve shall be a normal distribution. On the contrary, if the pore sizes are very different, then the distribution will be divided in two main intervals. This characteristic was mostly found in LFS samples, and in some ES samples with smaller fibre lengths and grammages.

The capillary rise of the paper substrates was next examined. Fluid transport in paper substrates obeys a $t^{1/2}$ dependency. Consequently, it can be described by the Washburn equation (Lucas 1918; Washburn 1921), as already demonstrated by Hodgson and Berg (1988). By fitting the shape of the water flow as a function of the square root of time, a linear relation for all studied paper substrates was obtained. As a result, the gradient of the curve can be determined and compared. Figure 4 shows the results of paper substrates made from LFS pulp with the same fibre length but at different grammages. It can be observed that all curves between 40 and 100 g/m^2 have a very similar gradient, whereas the curve with 20 g/m^2 has a lower gradient. The reason for this behaviour lies in two main aspects: first, the fibre layers forming the paper sheet are insufficient. That means that the cross-section area of the paper strip is very thin, so it limits the fluid transport by prolonging the wettability. Second, the void volume in the paper sheet is immense, which retards the fluid flow. In general, it can be emphasized that the grammage has no

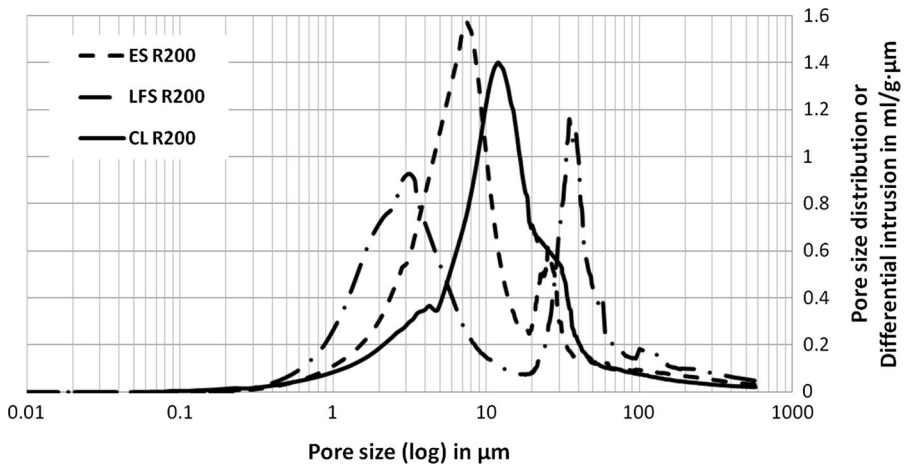

Fig. 3 Pore size distribution over pore size for eucalyptus sulphate (ES), long fibre mixture (LFS), and cotton linters (CL) at 80 g/m^2. Results determined by mercury porosimetry analysis

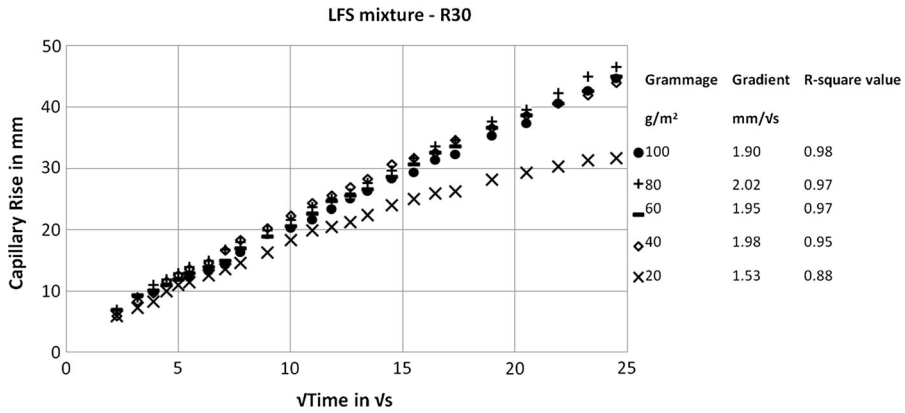

Fig. 4 Capillary rise over square root of time for paper substrates made of LFS with same fibre length at different grammages. Gradient and R-square value of each grammage

influence on the capillary rise. Furthermore, in order to achieve a continuous fluid flow, the grammage should be at least 40 g/m^2 or higher.

Contrary to Fig. 4, Fig. 5 shows the results of paper substrates made from LFS pulp with different fibre lengths at a constant grammage. It can be observed that each fraction has a diverse gradient. While longer fibres show a higher gradient, short fibres present a considerably much lower gradient, which was also achieved with unfractionated fibres. It is interesting to observe that the R200 fraction and the unfractionated sample present similar behaviour in the capillary rise. This can be explained due to the size of the fibres and the compact positioning of these in the paper sample. Porosity calculations confirmed an equal value of these two samples, while the others showed smaller values. This prevents the water from flowing at a higher speed.

Thus far the results for the capillary rise compared to the fibre length and grammage for LFS have been presented. Cotton linters, eucalyptus sulphate and groundwood were tested as well. Figure 6 illustrates the difference in the capillary rise between the four fibre types, plotted as the gradient as a function of the square root of time for various grammages. This diagram exemplifies the unfractionated fibre pulps, beaten until a freeness of 36 ± 1 SR was achieved. Overall, the four fibre types present the same behaviour, i.e. the gradient of the capillary rise declines as the grammage surges. However, CL shows the highest value, followed by ES, leaving LFS and GW with the smallest values. The low value of GW can be explained due to the higher lignin content, which slows down the capillary rise. In addition, further tests with unbleached samples, where the content of lignin is significantly higher than in bleached samples, established a notorious downward trend. It is important to point out that tests conducted with fractionated fibres, also show the same development.

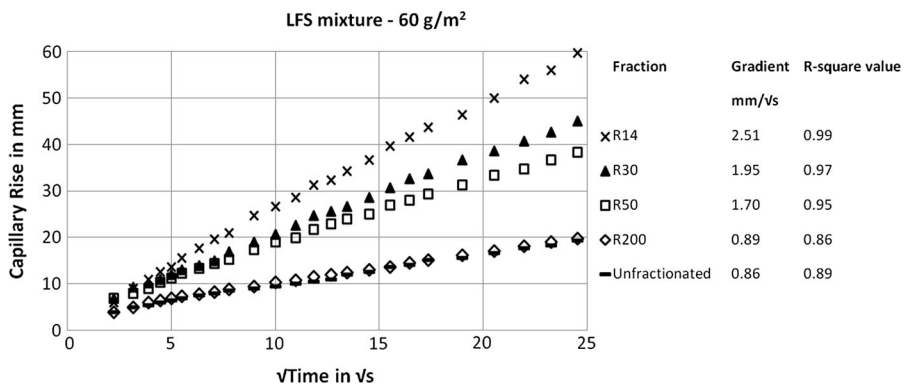

Fig. 5 Capillary rise over square root of time for paper substrates made of LFS with different fibre lengths at constant grammage. Gradient and R-square value of each fraction

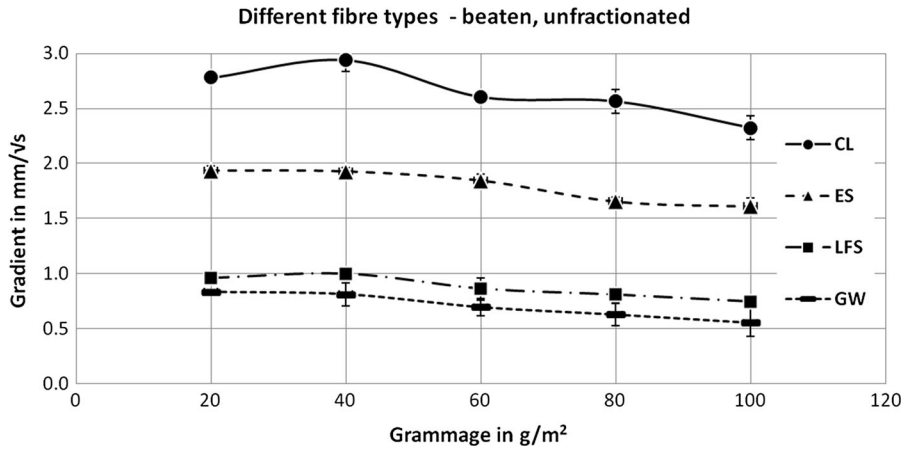

Fig. 6 Gradient of capillary rise over grammage for unfractionated CL, LFS, ES and GW with a freeness of 36 SR

Figure 7 shows overall differences and similarities between paper substrates with variable grammages, fibre lengths and orientations for cotton linters, as well as a comparison between lab-engineered paper substrates and commercially available filter paper. The columns plotted in Fig. 7 represent the gradient of the capillary rise as a function of the square root of time. From left to right, the first three columns establish that there are no significant changes in the gradient while increasing the grammage. This result also concurred with the results shown in Fig. 4. However, by fractionating the pulp and keeping the grammage constant, a change in the gradient can be achieved. Whereas the unfractionated sample shows a gradient of 2.35 mm/$\sqrt{s}$ (1st column), samples with defined fibre lengths lead to higher gradients (4th and 5th columns). An interesting fact is that anisotropic samples present a different gradient. Whilst paper substrates with fibres oriented in machine direction (MD) have a gradient of 2.41 mm/$\sqrt{s}$ (6th column), paper substrates with fibres oriented in cross direction (CD) have a gradient of 2.25 mm/$\sqrt{s}$ (7th column). In contrast to isotropic samples, both anisotropic samples have shown a higher gradient. Nevertheless, it is important to mention that anisotropic samples with diverse grammage have not shown any changes in the gradient, which also happened to be the case with isotropic samples. Lastly, it can be observed that commercial filter paper with fibres oriented in machine direction (9th column) presents a dramatic surge in the gradient with a value of

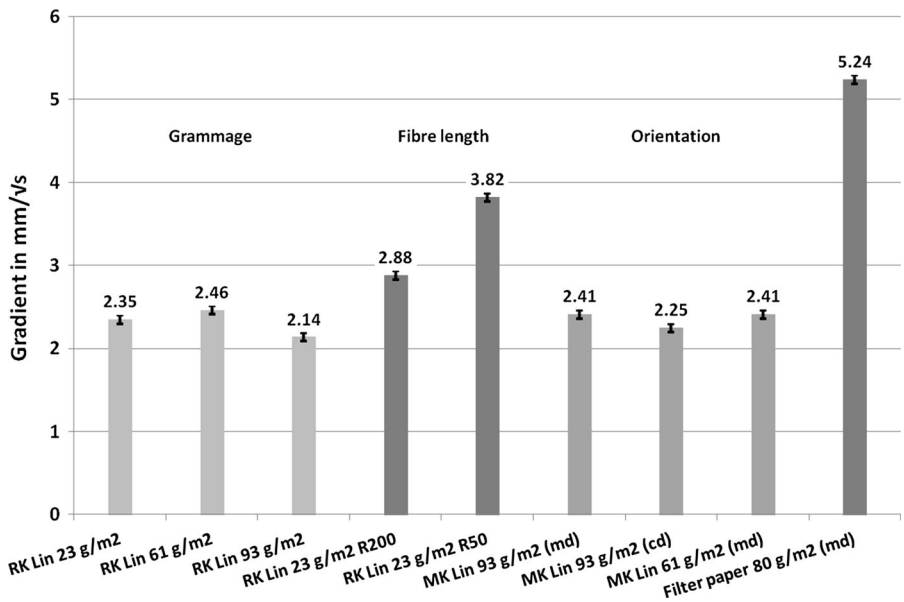

Fig. 7 Capillary rise of cotton linters paper substrates with different grammages, fibre lengths and fibre orientation, illustrated as the gradient in mm/$\sqrt{s}$. Filter paper in machine direction (MD)

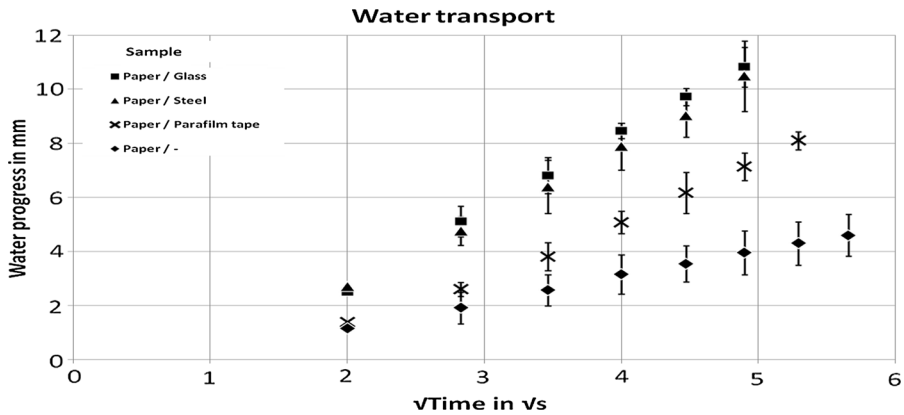

Fig. 8 Water progress over square root of time on a single paper strip, and on paper strips laid on glass, steel and Parafilm tape

5.24 mm/$\sqrt{s}$. Clearly, it can be stated that a wide variation in the capillary rise can be obtained by simply changing the length or orientation of the fibres, whereas the grammage has no considerable effect on the capillary rise.

Martinez et al. (2008) introduced a very ingenious and yet simple three-dimensional μPAD fabricated by stacking layers of patterned paper and double-sided adhesive tape. However, by placing paper samples in direct contact with other materials, the velocity in which the water flows through paper is instantly affected. Figure 8 shows the water progress over the square root of time, when paper strips are laid on glass, steel and Parafilm tape. Each material has a diverse water contact angle, which was previously mentioned in section "Determination of capillary rise". In addition, the water progress on a single paper strip was tested as a reference. It can be observed that each curve presents a different gradient. The single paper strip has the lowest gradient, whilst the other curves show a considerable increase in the gradient. These rises are inversely proportional to the contact angle, i.e., the Parafilm tape with the highest contact angle provides a lower value than steel and glass. However, between the steel and glass samples, only a slight difference in the water progress can be observed. This behaviour can be explained due to two reasons: first, by placing the two materials in contact, a small, additional porous layer between paper and testing material is created, allowing the water volume to increase; second, materials with a high contact angle are low wettable and therefore, the solid/liquid interactions are very weak, which results in the water being pushed away from the material, causing a fall in the water progress.

Conclusions

In the present study, fibres of cotton linters (CL), eucalyptus sulphate (ES), a mixture of 50 % pine sulphate and 50 % spruce sulphate (LFS), and groundwood (GW) were used to produce lab-engineered paper sheets. The characterization of the fibres for the specific component of the work of adhesion of several polar probes by inverse gas chromatography revealed several differences between CL and ES or LFS. Nevertheless, these differences could not be directly linked to the changes in the capillary rise. In contrast, notorious changes for the specific components of the works of adhesion (and for the surface energy) were established between GW and the bleached samples, suggesting a possible correlation with the capillary rise values: since the low capillary rise of GW is explained by the high lignin content and therefore by its surface properties and chemical composition.

On the other hand, the freeness value did present concrete influence on the capillary rise. Moreover, a correlation between the freeness value and specific surface area of fractionated and unfractionated fibre pulps was demonstrated.

Investigation of the porosity and pore size distribution of lab-engineered paper sheets revealed different values for several fibre types, when the freeness and the fibre length were kept constant. Apart from that, the porosity decreased its value as the grammage increased.

Different approaches to modulate and control fluid transport in lab-engineered paper substrates were also introduced by only using different fibre types with the same freeness value. In addition, a different behaviour of the fluid transport is presented, when lab-

engineered paper substrates are made with fibres, which have been previously fractionated. In contrast, we showed that the grammage has no influence on the fluid transport in paper substrates. Our studies also showed that the fluid transport can be altered, by changing the orientation of the fibres. Both, fibres aligned in machine direction or cross direction increased the fluid transport; however, the former provided a higher value. A comparison of lab-engineered paper substrates with commercially available filter paper showed notorious differences in the fluid transport. Even though filter paper managed to achieve a higher capillary rise, it failed to provide alternatives to manipulate the fluid flow.

Finally, we investigated changes in the fluid transport in paper substrates, when they were put in contact with other materials. This results in an increment of the fluid transport. Furthermore, high wettable materials with a contact angle below 90° showed an even higher rise in the fluid transport.

Acknowledgments F. Carstens would like to thank the "National Council of Science and Technology, CONACYT" and the "German Academic Exchange Service, DAAD" for a research scholarship.

References

Abe K, Suzuki K, Citterio D (2008) Inkjet-printed microfluidic multianalyte chemical sensing paper. Anal Chem 80:6928–6934. doi:10.1021/ac800604v

Abe K, Kotera K, Suzuki K, Citterio D (2010) Inkjet-printed paperfluidic immuno-chemical sensing device. Anal Bioanal Chem 398:885–893. doi:10.1007/s00216-010-4011-2

Bal K, Fan J, Sarkar MK, Ye L (2011) Differential spontaneous capillary flow through heterogeneous porous media. Int J Heat Mass Transf 54:3096–3099. doi:10.1016/j.ijheatmasstransfer.2011.02.048

Böhm A, Carstens F, Trieb C, Schabel S, Biesalski M (2014) Engineering microfluidic papers: effect of fiber source and paper sheet properties on capillary-driven fluid flow. Microfluid Nanofluid 16:789–799. doi:10.1007/s10404-013-1324-4

Bruzewicz DA, Reches M, Whitesides GM (2008) Low-cost printing of poly(dimethylsiloxane) barriers to define microchannels in paper. Anal Chem 80:3387–3392. doi:10.1021/ac702605a

Cai J, Yu B, Zou M, Luo L (2010) Fractal characterization of spontaneous co-current imbibition in porous media. Energy Fuels 24:1860–1867

Carman PC (1937) Fluid flow through granular beds. Trans Inst Chem Eng 15:150–166

Carman PC (1956) Flow of gases through porous media. Academic Press, New York

Carrilho E, Martinez AW, Whitesides GM (2009) Understanding wax printing: a simple micropatterning process for paper-based microfluidics. Anal Chem 81:7091–7095. doi:10.1021/ac901071p

Carvalho MG, Santos JMRCA, Martins AA, Figueiredo MM (2005) The effects of beating, web forming and sizing on the surface energy of eucalyptus globulus kraft fibres evaluated by inverse gas chromatography. Cellulose 12:371–383

Cate DM, Adkins JA, Mettakoonpitak J, Henry CS (2015) Recent developments in paper-based microfluidic devices. Anal Chem 87:19–41. doi:10.1021/ac503968p

Chitnis G, Ding Z, Chang C-L, Savran CA, Ziaie B (2011) Laser-treated hydrophobic paper: an inexpensive microfluidic platform. Lab Chip 11:1161–1165. doi:10.1039/C0LC00512F

Davy J (1812) On a gaseous compound of carbonic oxide and chlorine. Philos Trans R Soc Lond 102:144–151

Delaney JL, Hogan CF, Tian J, Shen W (2011) Electrogenerated chemiluminescence detection in paper-based microfluidic sensors. Anal Chem 83:1300–1306. doi:10.1021/ac102392t

Dungchai W, Chailapakul O, Henry CS (2011) A low-cost, simple, and rapid fabrication method for paper-based microfluidics using wax screen-printing. The Analyst 136:77–82. doi:10.1039/c0an00406e

Erbil Y (1997) Calculation of spreading pressure of water on cellulosic films from contact angle data. J Chem 21:332–345

Fang L, Jiang J, Wang J, Deng C (2014) Non-uniform capillary model for unidirectional fiber bundles considering pore size distribution. J Reinf Plast Compos 33:1430–1440. doi:10.1177/0731684414533739

Fenton EM, Mascarenas MR, Lopez GP, Sibbett SS (2009) Multiplex lateral-flow test strips fabricated by two-dimensional shaping. ACS Appl Mater Interfaces 1:124–129. doi:10.1021/am800043z

Fu E, Lutz B, Kauffman P, Yager P (2010) Controlled reagent transport in disposable 2D paper networks. Lab Chip 10:918–920. doi:10.1039/b919614e

Fu E, Ramsey SA, Kauffman P, Lutz B, Yager P (2011) Transport in two-dimensional paper networks. Microfluid Nanofluid 10:29–35. doi:10.1007/s10404-010-0643-y

Gamelas JAF (2013) The surface properties of cellulose and lignocellulosic materials assessed by inverse gas chromatography: a review. Cellulose 20:2675–2693. doi:10.1007/s10570-013-0066-5

Gamelas JAF, Santos JMRCA, Ferreira PJ (2011) Surface energetics of softwood kraft pulps by inverse gas chromatography. In: Ander P, Bauer W, Heinemann S, Kallio P, Passas, R, Treimanis A (eds) Fine structure of papermaking fibres—the final report of COST Action E54, Brussels, pp 39–49

Gamelas JAF, Ferraz E, Rocha F (2014) An insight into the surface properties of calcined kaolinitic clays: the grinding effect. Colloids Surf A 455:49–57. doi:10.1016/j.colsurfa.2014.04.038

Giesche H (2006) Mercury porosimetry: a general (practical) overview. Part Part Syst Charact 23:9–19. doi:10.1002/ppsc.200601009

Guan LY, Tian JF, Cao R, Li MS, Cai ZX, Shen W (2014) Barcode-like paper sensor for smartphone diagnostics: an application of blood typing. Anal Chem 86:11362–11367

Hodgson KT, Berg JC (1988) The effect of surfactants on wicking flow in fiber networks. J Colloid Interface Sci 121:22–31. doi:10.1016/0021-9797(88)90404-3

Hubbe MA, Gardner DJ, Shen W (2015) Contact angles and wettability of cellulosic surfaces: a review of proposed mechanisms and test strategies. BioResources 10:8657–8749

Johansson A (2011) Correlation between fibre properties and paper properties. University of Oregon, Eugene, pp 1–49

Joubert JM, Krige GJR, Borgin K (1959) Evidence for a hydrate of cellulose from studies of its surface properties. Nature 184:1561–1562

Kämäräinen T et al (2016) UV-ozone patterning of micro-nano fibrillated cellulose (MNFC) with alkylsilane self-assembled monolayers. Cellulose 23:1847–1857. doi:10.1007/s10570-016-0942-x

Kamdem DP, Riedl B (1992) Inverse gas chromatography of lignocellulosic fibers coated with a thermosetting polymer: use of peak maximum and conder and young methods. J Colloid Interface Sci 150:507–516. doi:10.1016/0021-9797(92)90219-C

Kargl R, Mohan T, Köstler S, Spirk S, Doliška A, Stana-Kleinschek K, Ribitsch V (2013) Functional patterning of biopolymer thin films using enzymes and lithographic methods. Adv Funct Mater 23:308–315. doi:10.1002/adfm.201200607

Kozeny J (1927) Über kapillare Leitung des Wassers im Boden. Wien 136:271–306

León y León CA (1998) New perspectives in mercury porosimetry. Adv Colloid Interface Sci 76–77:341–372

Li X, Tian J, Nguyen T, Shen W (2008) Paper-based microfluidic devices by plasma treatment. Anal Chem 80:9131–9134. doi:10.1021/ac801729t

Li X, Tian J, Garnier G, Shen W (2010) Fabrication of paper-based microfluidic sensors by printing. Colloids Surf B Biointerfaces 76:564–570. doi:10.1016/j.colsurfb.2009.12.023

Li X, Ballerini DR, Shen W (2012) A perspective on paper-based microfluidics: current status and future trends. Biomicrofluidics 6:1–13. doi:10.1063/1.3687398

Li LZ, Huang XL, Liu W, Shen W (2014) Control performance of paper-based blood analysis devices through paper structure design. ACS Appl Mater Interfaces 6:21624–21631

Liukkonen A (1997) Contact angle of water on paper components: sessile drops versus environmental scanning electron microscope measurements. Scanning 19:411–415

Lu Y, Shi W, Qin J, Lin B (2010) Fabrication and characterization of paper-based microfluidics prepared in nitrocellulose membrane by wax printing. Anal Chem 82:329–335

Lucas R (1918) Ueber das Zeitgesetz des kapillaren Aufstiegs von Flüssigkeiten. Kolloid-Zeitschrift 23:15–22. doi:10.1007/bf01461107

Lutz B, Liang T, Fu E, Ramachandran S, Kauffman P, Yager P (2013) Dissolvable fluidic time delays for programming multi-step assays in instrument-free paper diagnostics. Lab Chip 13:2840–2847

Mark A et al (2012) Multi-scale simulation of paperboard edge wicking using a fiber-resolving virtual paper model. Tappi J 11:9–16

Martinez AW, Phillips ST, Butte MJ, Whitesides GM (2007) Patterned paper as a platform for inexpensive, low-volume, portable bioassays. Angew Chem Int Ed Engl 46:1318–1320. doi:10.1002/anie.200603817

Martinez AW, Phillips ST, Whitesides GM (2008) Three-dimensional microfluidic devices fabricated in layered paper and tape. Proc Natl Acad Sci USA 105:19606–19611. doi:10.1073/pnas.0810903105

Masoodi R, Pillai KM, Varanasi PP (2007) Darcy's law-based models for liquid absorption in polymer wicks. Am Inst Chem Eng 53:2769–2782. doi:10.1002/aic.11322

Masoodi R, Pillai KM, Varanasi PP (2010) Effect of externally applied liquid pressure on wicking in paper wipes. J Eng Fibers Fabr 5:49–66

Micromeritics (2015) AutoPore IV Series—mercury porosimeters. Micromeritics Instrument Corp, Norcross, pp 1–6

Mukhopadhyay P, Schreiber HP (1995) Aspects of acid-base interactions and use of inverse gas chromatography. Colloids Surf A 100:47–71. doi:10.1016/0927-7757(95)03137-3

Müller RH, Clegg DL (1949) Automatic paper chromatography. Anal Chem 21:1123–1125

Nguyen TH, Fraiwan A, Choi S (2014) Paper-based batteries: a review. Biosens Bioelectron 54:640–649

Nilghaz A, Zhang L, Shen W (2015) Coffee stains on paper. Chem Eng Sci 129:34–41. doi:10.1016/j.ces.2015.02.017

Niskanen K (1998) Paper physics. Papermaking science and technology, book 16. Fapet Oy, Helsinki, pp 1–162

Olkkonen J, Lehtinen K, Erho T (2010) Flexographically printed fluidic structures in paper. Anal Chem 82:10246–10250. doi:10.1021/ac1027066

Patro D, Bhattacharyya S, Jayaram V (2007) Flow kinetics in porous ceramics: understanding with non-uniform capillary models. J Am Ceram Soc 90:3040–3046. doi:10.1111/j.1551-2916.2007.01776.x

Poiseuille JLM (1828) Recherches sur la force du coeur aortique. Doctoral Thesis, pp 1–46

Reutenauer S, Thielmann F (2003) The characterization of cotton fibers and the interaction with perfume molecules by inverse gas chromatography (IGC). J Mater Sci 38:2205–2208

Reyssat M, Courbin L, Reyssat E, Stone HA (2008) Imbibition in geometries with axial variations. J Fluid Mech 615:335–344. doi:10.1017/s0022112008003996

Robertson AA, Mason SG (1949) Specific surface of cellulose fibers by the liquid permeability method. Pulp Paper Mag Can 50:103–110

Rudman I, Patterson TF (1998) Water and air permeability of wet sheets. Prog Rep 6:1–44

Santos JMRCA, Guthrie JT (2005) Analysis of interactions in multicomponent polymeric systems: the key-role of inverse gas chromatography. Mater Sci Eng, R 50:79–107

Schultz J, Lavielle L, Martin C (1987) The role of the interface in carbon fibre-epoxy composites. J Adhes 23:45–60. doi:10.1080/00218468708080469

Shen W, Parker IH (1999) Surface composition and surface energetics of various eucalypt pulps. Cellulose 6:41–55

Shen W, Parker IH, Sheng YJ (1998) The effects of surface extractives and lignin on the surface energy of eucalypt kraft pulp fibers. J Adhes Sci Technol 12:161–174

Shou D, Ye L, Fan J, Fu K (2014) Optimal design of porous structures for the fastest liquid absorption. Langmuir 30:149–155. doi:10.1021/la4034063

Sieb N (2015) Mercury porosimeter—standard operating procedure, 4D LABS, Revision 3.0, pp 1–17

Singh R (2007) The saturated permeability of composite pulp fiber and filler mats. ProQuest, Ann Arbor

Szekely J, Neumann AW, Chuang YK (1971) The rate of capillary penetration and the applicability of the Washburn equation. J Colloid Interface Sci 35:273–278. doi:10.1016/0021-9797(71)90120-2

Taudte RV, Beavis A, Wilson-Wilde L, Roux C, Doble P, Blanes L (2013) A portable explosive detector based on fluorescence quenching of pyrene deposited on coloured wax-printed μPADs. Lab Chip 13:4164–4172

Tobjörk D, Österbacka R (2011) Paper electronics. Adv Mater 23:1935–1961

Topalovic T, Nierstrasz, VA, Bautista, L, Jocic D, Navarro A, Warmoeskerken, MMCG (2007) Analysis of the effects of catalytic bleaching on cotton. Cellulose 14:385–400

Wang W, Wu WY, Wang W, Zhu JJ (2010) Tree-shaped paper strip for semiquantitative colorimetric detection of protein with self-calibration. J Chromatogr A 1217:3896–3899. doi:10.1016/j.chroma.2010.04.017

Washburn EW (1921) The dynamics of capillary flow. Phys Rev 17:273–283. doi:10.1103/PhysRev.17.273

Webb PA (2001) An introduction to the physical characterization of materials by mercury intrusion porosimetry with emphasis on reduction and presentation of experimental data. Micromeritics Instrument Corp, Norcross, pp 1–23

Wistara N, Young RA (1999) Properties and treatments of pulps from recycled paper. Part I. Physical and chemical properties of pulps. Cellulose 6:291–324

Xiao J, Stone HA, Attinger D (2012) Source-like solution for radial imbibition into a homogeneous semi-infinite porous medium. Langmuir 28:4208–4212